IEICE TRANS. COMMUN., VOL.E98–B, NO.12 DECEMBER 2015

PAPER

Supervised SOM Based ATR Method with Circular Polarization Basis of Full Polarimetric Data

Shouhei OHNO[†], **Shouhei KIDERA**[††a)], ***and*** **Tetsuo KIRIMOTO**[††], ***Members***

SUMMARY Satellite-borne or aircraft-borne synthetic aperture radar (SAR) is useful for high resolution imaging analysis for terrain surface monitoring or surveillance, particularly in optically harsh environments. For surveillance application, there are various approaches for automatic target recognition (ATR) of SAR images aiming at monitoring unidentified ships or aircraft. In addition, various types of analyses for full polarimetric data have been developed recently because it can provide significant information to identify structure of targets, such as vegetation, urban, sea surface areas. ATR generally consists of two processes, one is target feature extraction including target area determination, and the other is classification. In this paper, we propose novel methods for these two processes that suit full polarimetric exploitation. As the target area extraction method, we introduce a peak signal-to noise ratio (PSNR) based synthesis with full polarimetric SAR images. As the classification method, the circular polarization basis conversion is adopted to improve the robustness especially to variation of target rotation angles. Experiments on a 1/100 scale model of X-band SAR, demonstrate that our proposed method significantly improves the accuracy of target area extraction and classification, even in noisy or target rotating situations.

key words: *synthetic aperture radar (SAR), polarimetric SAR, automatic target recognition (ATR), target area extraction, circular polarization basis*

1. Introduction

Microwave radar is one of the most useful techniques for measuring ground terrain or sea surface, even in optically unclarity situations such as adverse weather or darkness. Synthetic aperture radar (SAR) is the most well-known microwave imaging method that has been applied to earth observation for environmental monitoring or for maritime security with regard to the identification of ships or aircrafts, because it can provide high-resolution and complex-valued images. However, it is still difficult for an inexperienced operator to recognize targets within SAR imagery compared with optical images, because SAR images are generated by radio signals with wavelengths of the order of centimeters.

To address this issue, various types of automatic target recognition (ATR) approaches have been developed in recent years, which include machine learning methods such as neural networks [1] or support vector machine (SVM) [2]. In particular, there have been many reports stating that neural-network-based classification retains a certain level of accuracy in target recognition with SAR imagery. However, such approaches result in seriously degraded classification accuracy when the available SAR images are highly contaminated by random noise. To overcome this difficulty, we have previously proposed the ATR method based on a supervised self-organizing map (SOM) method, where the unified distance matrix (U-matrix) metric is employed in the classification stage [3]. This method has been demonstrated to enhance the ATR performance remarkably compared with that obtained by major neural network or SVM-based approaches because it assesses not only differences in output from training and test inputs, but also the potential barrier generated by the U-matrix metric.

It should be noted that this method only deals with single polarimetric SAR data. As suggested in various studies, full polarimetric SAR data have great potential for improving ATR performance [4]. There are many studies on full polarimetric SAR analysis that focus on structure recognition such as the ground surface, paddy fields, forests, or artificial buildings [5]. These studies have also indicated that the recognition accuracy significantly depends on the feature extraction method, especially regarding to the performance of target area extraction. As one of the most effective target area extraction methods, the polarimetric whitening filter (PWF) method has been developed to eliminate a speckle noise from SAR images [6]. While this method suppresses highly correlated speckle noise among different polarimetric SAR images, it has been reported that this method was not oriented to suppress a receiver white noise (not correlated noise), and suffered from an inaccuracy due to suppressing correlated target components. To overcome the above problem, this paper first proposes a novel method for target area extraction, which synthesizes full polarimetric SAR images weighted by peak signal-to-noise ratio (PSNR) to consider the SNR imbalance among each SAR image.

As to classification issue, this paper also extends the conventional SOM based ATR method [3] to be suitable for full polarimetric data, where the dimension of input vector is simply trebled. Furthermore, the conventional method suffers from inaccuracy for classification, where an unknown input image has different azimuth angle from the training image, namely, in target rotating situation. There is the extended method to deal with this problem, where multi training data with different azimuth angle are preliminary learned in SOM [7]. However, it requires more training data and larger SOM neurons. To overcome this difficulty, this paper also introduces the rotation angle compensation method

Manuscript received April 2, 2015.
Manuscript revised August 18, 2015.

[†]The author is with NEC Corpolation, Fuchu-shi, 183-8501 Japan.
[††]The authors are with Graduate School of Informatics and Engineering, The University of Electro-Communications, Chofu-shi, 182-8585 Japan.
a) E-mail: kidera@ee.uec.ac.jp

DOI: 10.1587/transcom.E98.B.2520

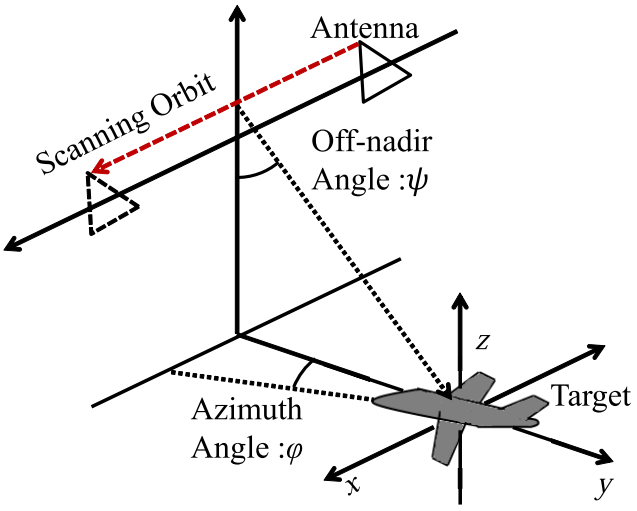

Fig. 1 System model.

and employs the circular polarization basis conversion. The literature [8] reports that the power ratio of circular polarization component is invariant for target rotation regardless of target structure, and it is suitable for dealing with the above problem.

The experimental data, obtained in assuming the 1/100-scale model of an X-band SAR, demonstrate that the proposed method significantly improves the target area extraction performance, even in lower PSNR situation and also enhances classification accuracy by using circular polarization basis, where the target aircraft has a different azimuth angle.

2. System Model

Figure 1 shows the geometry of the observation model. It assumes a mono-static radar, where a set of transmitting and receiving antennas is scanned along the straight line as $y = y_0, z = z_0$. The target is located on the plane at $z = 0$, the off-nadir angle is ψ. The target rotates along the z axis, and its rotation angle (called azimuth angle) is denoted by ϕ. The two linear polarizations are assumed as the vertical (denoted by V) and horizontal (denoted by H) directions in the transmitting and receiving antennas. Then, the full combination of polarimetric data as VV, VH, HV, and HH are obtained (e.g., VH denotes vertical polarization in transmitting and horizontal polarization in receiving). Here, it assumes the reciprocity as HV = VH. The polarimetric SAR complex image, focused on the $z = 0$ plane, is defined as $S_{ij}(x, y)$, where the subscripts i and j denote H or V.

3. Conventional Method

We have already proposed the efficient ATR method based on the supervised SOM and the U-matrix metric [3]. This section briefly describes the methodology of this method, because it is basis of our proposed method. First, in the learning process, the SOM is generated with reliable SAR images as training data, where the reliable SAR image denotes an image with a sufficiently high SNR. The SOM map consists of $M_x \times M_y$ nodes (neurons). To remove the speckle or random noise, the SAR images are binarized as;

$$I^{\mathrm{bi}}(x, y) = \begin{cases} 1\ (|S(x, y)| \geq I_{\mathrm{th}}), \\ 0\ (\text{Otherwise}), \end{cases} \tag{1}$$

where the threshold I_{th} is defined by Otsu's discriminant analysis [9]. The SAR image vector is set as

$$\boldsymbol{x} = [I^{\mathrm{bi}}(x_1, y_1), \cdots, I^{\mathrm{bi}}(x_{N_x}, y_{N_y})], \tag{2}$$

where N_x, N_y are the total numbers of pixels for the x and y axes. The training SAR images are defined as $\boldsymbol{x}_k^{\mathrm{tr}}, (k = 1, 2, \cdots, N_{\mathrm{tr}})$. The location of each node is denoted by $\boldsymbol{p}$, and the node has an output image defined as $\boldsymbol{y}(\boldsymbol{p}; t)$, where t is the number of training trials. An initial output $\boldsymbol{y}(\boldsymbol{p}; 0)$ for each node is defined using a linear mixture of the training images. Next, for the k-th training data $\boldsymbol{x}_k^{\mathrm{tr}}$, the location of the winner node $\hat{\boldsymbol{p}}_k(t)$ is determined as

$$\hat{\boldsymbol{p}}_k(t) = \underset{\boldsymbol{p} \in \mathcal{P}}{\operatorname{argmin}} \left\| \boldsymbol{y}(\boldsymbol{p}; t) - \boldsymbol{x}_k^{\mathrm{tr}} \right\|. \tag{3}$$

Here, $\mathcal{P}$ denotes an entire set of nodes on SOM. After calculating $\hat{\boldsymbol{p}}_k(t)$ for all the training data, the output of each node is updated by:

$$\boldsymbol{y}(\boldsymbol{p}; t+1) = \boldsymbol{y}(\boldsymbol{p}; t) + \beta(t) \frac{\sum_{k=1}^{N_{\mathrm{tr}}} h(\hat{\boldsymbol{p}}_k(t), \boldsymbol{p})(\boldsymbol{x}_k^{\mathrm{tr}} - \boldsymbol{y}(\boldsymbol{p}; t))}{\sum_{k=1}^{N_{\mathrm{tr}}} h(\hat{\boldsymbol{p}}_k(t), \boldsymbol{p})}, \tag{4}$$

where $h(\hat{\boldsymbol{p}}_k(t), \boldsymbol{p})$ is the neighboring function as

$$h(\hat{\boldsymbol{p}}_k(t), \boldsymbol{p}) = \exp\left(-\frac{\|\hat{\boldsymbol{p}}_k(t) - \boldsymbol{p}\|}{2\sigma(t)^2} \right). \tag{5}$$

Here, t is training trials ($t = 1, 2, \cdots, \mathrm{T_{som}}$), $\mathrm{T_{som}}$ denotes the total number of training trials, $\beta(t)$ and $\sigma(t)$ are monotonically decreasing functions for t. The batch learning (BL) approach [10] is introduced so that the obtained SOM should be robust against the order of the training data sequence. Furthermore, to assess the entire region of the SOM under a fair standard, the periodical structure of SOM is considered as in [11]; these are classified as torus-type SOMs. Finally, the U-matrix potential field is generated by the final SOM [12].

In the classification process, this method employs topological U-matrix features of SOM, namely, for unknown image $\boldsymbol{x}$, the following metric is assessed,

$$R_k^{\mathrm{som}} = \min_{C(\boldsymbol{x}_k^{\mathrm{tr}}, \boldsymbol{x})} \int_{C(\boldsymbol{x}_k^{\mathrm{tr}}, \boldsymbol{x})} U(\boldsymbol{p}) \mathrm{d}\boldsymbol{p}, \tag{6}$$

where $\boldsymbol{p}$ denotes the position of the U-matrix field and $C(\boldsymbol{x}_k^{\mathrm{tr}}, \boldsymbol{x})$ denotes all possible paths from $\hat{\boldsymbol{p}}_k(\mathrm{T_{som}})$ to $\hat{\boldsymbol{p}}(\boldsymbol{x})$ for Manhattan distance, where $\hat{\boldsymbol{p}}(\boldsymbol{x})$ denotes the winner node for $\boldsymbol{x}$. Here, the path integral of Eq. (6) is calculated by A-star algorithm to reduce the calculation amount [7]. $U(\boldsymbol{p})$ is the U-matrix value on $\boldsymbol{p}$, $\hat{\boldsymbol{p}}_k(\mathrm{T_{som}})$ expresses each winner

node for the k-th training data and $\hat{\boldsymbol{p}}(\boldsymbol{x})$ is the winner node of the unknown input, which is determined in the same way as learning process. The unknown image $\boldsymbol{x}$ is classified into the k th training image $\boldsymbol{x}_k^{\mathrm{tr}}$ when the R_k^{som} becomes minimum in all training images.

It has been reported that this method significantly enhanced the recognition accuracy compared with obtained by the neural network approach, by exploiting the feature of U-matrix field [3]. However, this method suffers from the degradation of recognition performance, where an unknown target image has a different azimuth angle of the training data. While the extension of this method has been proposed by increasing the training data with different azimuth angles, it needs more training process or data and requires sufficiently large SOM neurons [7].

4. Proposed Method

To overcome the problem mentioned in Sect. 3, this paper proposes a novel method by exploiting full polarimetric data, to achieve more accurate and robust ATR performance. First, the target area extraction is proposed to suppress the additive noise in SAR image by considering SNR imbalance among HH, VV and HV components. Next, to deal with the angular varied situations, the proposed method introduces the rotation angle compensation method and employs the circular polarization basis conversion when the training data with one azimuth angle is only input to the SOM.

4.1 Target Area Extraction Method

As one of the most useful methods for dealing with full polarimetric data in the ATR issue, the PWF has been proposed [6]. This method enhances target area extraction accuracy by adopting the decorrelating conversion among different polarimetric SAR images, which contributes to suppressing speckle noise in SAR images. However, this method suffers from inaccuracies in target area extraction because it also suppresses the correlated target signals among different polarization, and does not consider the SNR imbalance for target area extraction.

To address this problem, this paper synthesizes each polarimetric SAR image weighted by the PSNR as;

$$P_{\mathrm{full}}(x,y) = \hat{\sigma}_{\mathrm{HH}}\langle|S_{\mathrm{HH}}|^2\rangle + 2\hat{\sigma}_{\mathrm{HV}}\langle|S_{\mathrm{HV}}|^2\rangle + \hat{\sigma}_{\mathrm{VV}}\langle|S_{\mathrm{VV}}|^2\rangle, \tag{7}$$

where $\langle * \rangle$ denotes a spatial averaging, and $\hat{\sigma}_{ij}(i,j = \mathrm{H},\mathrm{V})$ expresses the normalized PSNR defined as

$$\hat{\sigma}_{ij} = \frac{\sigma_{ij}}{\sigma_{\mathrm{HH}} + 2\sigma_{\mathrm{HV}} + \sigma_{\mathrm{VV}}}. \tag{8}$$

Here, each σ_{ij} denotes PSNR as;

$$\sigma_{ij} = \frac{\max_{x,y\in\Omega}\langle|S_{ij}(x,y)|^2\rangle}{\mathrm{mean}_{x,y\in\Omega_{\mathrm{N}}}\langle|S_{ij}(x,y)|^2\rangle}, \tag{9}$$

where Ω denotes the entire area of the image, Ω_{N} denotes the focused area by signals including only receiver noises. Then, the target area denoted as Ω_{tar} is determined as;

$$\Omega_{\mathrm{tar}} = \{(x,y) \in \Omega \mid P_{\mathrm{full}}(x,y) \geq P_{\mathrm{th}}\}, \tag{10}$$

where P_{th} denotes the threshold, preliminarily determined.

4.2 Azimuth Angle Compensation

This subsection explains the extension of the conventional ATR method [3] to full polarimetric SAR images to enhance the robustness against the target azimuth rotation. First, as a preprocessing, this paper introduces the azimuth angle compensation method. The azimuth direction ϕ of unknown image is estimated as

$$\hat{\phi} = \underset{-\frac{\pi}{2}\leq\phi\leq\frac{\pi}{2}}{\arg\max} \frac{\sum_{x,y} P^{\mathrm{bi}}(x,y)P^{\mathrm{bi}}_{\mathrm{ref}}(x,y,\phi)}{\sqrt{\sum_{x,y} P^{\mathrm{bi}}(x,y)^2}\sqrt{\sum_{x,y} P^{\mathrm{bi}}_{\mathrm{ref}}(x,y,\phi)^2}}, \tag{11}$$

where $P^{\mathrm{bi}}(x,y)$ is the binarized image of feature value $P_{\mathrm{full}}(x,y)$ defined as;

$$P^{\mathrm{bi}}(x,y) = \begin{cases} 1 & (P_{\mathrm{full}}(x,y) \geq \hat{P}_{\mathrm{th}}) \\ 0 & (\mathrm{Otherwise}) \end{cases}, \tag{12}$$

where the threshold $\hat{P}_{\mathrm{th}}$ is automatically determined by Otsu's discriminant analysis [9]. $P^{\mathrm{bi}}_{\mathrm{ref}}(x,y,\phi)$ denotes the image rotating the reference image $P^{\mathrm{bi}}_{\mathrm{ref}}(x,y)$ with ϕ around the target center point.

4.3 Feature Value Extension for Full Polarimetric Data

Next, the feature value of training and unknown images is extended to full polarimetric data. Although the full polarimetric data, in general, is observed from the linear polarization (LP) basis, it has been reported that the power ratio of the LP components varies due to the target rotation [8]. This variations become critical for ATR performance in the method [3], because it compares spatial distribution of the power for each polarization SAR image as in Eq. (3). On the contrary, it has been found that the power ratio of circular polarization (CP) component is invariant for target rotation in [13]. Thus, this paper introduces the CP basis to maintain the ATR performance for target rotation. The scattering matrix of the LP basis is transformed to that of CP basis as;

$$\boldsymbol{S}_{\mathrm{CP}}(x,y) = \begin{bmatrix} S_{\mathrm{LL}}(x,y) & S_{\mathrm{LR}}(x,y) \\ S_{\mathrm{RL}}(x,y) & S_{\mathrm{RR}}(x,y) \end{bmatrix} = \frac{1}{2}\begin{bmatrix} 1 & \mathrm{j} \\ \mathrm{j} & 1 \end{bmatrix}\begin{bmatrix} S_{\mathrm{HH}}(x,y) & S_{\mathrm{HV}}(x,y) \\ S_{\mathrm{VH}}(x,y) & S_{\mathrm{VV}}(x,y) \end{bmatrix}\begin{bmatrix} 1 & \mathrm{j} \\ \mathrm{j} & 1 \end{bmatrix}, \tag{13}$$

where the subscripts L and R denote the left-handed and right-handed circular polarizations, respectively. Then, the proposed method introduces the feature values $\boldsymbol{Z}_{\mathrm{CP}}$ for training and unknown data as

$$\boldsymbol{Z}_{\mathrm{CP}} = \frac{[z_{\mathrm{LL}}, 2z_{\mathrm{LR}}, z_{\mathrm{RR}}]}{\max_{x,y\in\Omega}(z_{\mathrm{LL}} + 2z_{\mathrm{LR}} + z_{\mathrm{RR}})}. \tag{14}$$

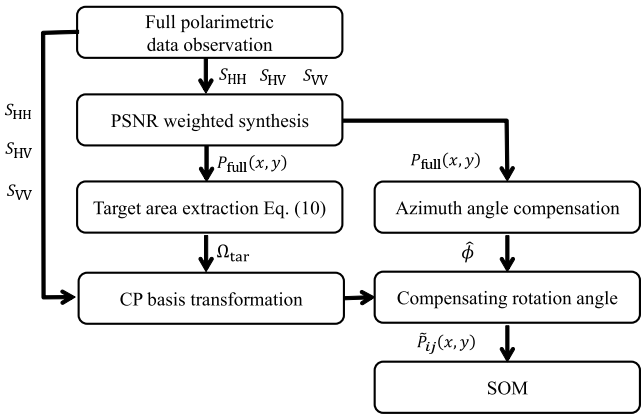

Fig. 2 Flowchart of the proposed method.

Ω is the entire area of the SAR image. Here, the SAR image vector $z_{ij}(i = \mathrm{L}\text{ or }\mathrm{R}, j = \mathrm{L}\text{ or }\mathrm{R})$ is determined as;

$$\begin{aligned} z_{ij} = \big[&\tilde{P}_{ij}(x_1, y_1), \cdots, \tilde{P}_{ij}(x_1, y_{N_y}), \\ &\tilde{P}_{ij}(x_2, y_1) \cdots, \tilde{P}_{ij}(x_2, y_{N_y}), \\ &\cdots, \\ &\tilde{P}_{ij}(x_{N_x}, y_1) \cdots, \tilde{P}_{ij}(x_{N_x}, y_{N_y})\big], \end{aligned} \tag{15}$$

where N_x and N_y denote the total number of pixels along the x and y axes. Here, $\tilde{P}_{ij}(x, y)$ is defined as;

$$\tilde{P}_{ij}(x,y) = \begin{cases} \langle |S_{ij}(x,y)|^2 \rangle & ((x,y) \in \Omega_{tar}) \\ 0 & (\text{Otherwise}) \end{cases}. \tag{16}$$

Ω_{tar} is determined as in Eq. (10).

Finally, the actual procedure of the proposed method is summarized as follows.

Step 1)
$P_{full}(x, y)$ is calculated in Eq. (7) and the target area Ω_{tar} is extracted as in Eq. (10).

Step 2)
Using binalized feature of $P_{full}(x, y)$, the azimuth rotating angle ϕ is estimated in Eq. (11) as $\hat{\phi}$.

Step 3)
$\boldsymbol{S}_{CP}$ is generated from the observed LP basis SAR images as in Eq. (13) in the area of Ω_{tar}, $\tilde{P}_{ij}(x, y)$ is determined in Eq. (16).

Step 4)
$\tilde{P}_{ij}(x, y)$ is rotated along the target center point with the estimated azimuth angle as $\hat{\phi}$.

Step 4)
Feature value $\boldsymbol{Z}_{CP}$ is generated in Eq. (14), and the SOM is trained with $\boldsymbol{Z}_{CP}$, where only the training data with $\phi = 0$ are used.

Step 5)
For unknown input, the process from Step 1) to Step 4) is carried out, and $\boldsymbol{Z}_{CP}$ for unknown input is classified with the learned SOM using U-matrix metric.

Figure 2 shows the flowchart of the proposed method.

5. Performance Evaluation with Experimental Data

This section describes the two types of performance evaluation for the proposed method in terms of the target area extraction and the ATR performance through experimental data. This experiment assumes about the 1/100-scale model of a typical X-band SAR system, except for the center frequency. Figure 3 shows the experimental setup. Here, the off-nadir angle ψ is 65°, the height of the antenna is 1.14 m, frequency is swept from 26 GHz to 40 GHz, and synthetic aperture length is 1.6 m. The azimuth direction of targets is defined as ϕ in Fig. 1. The theoretical range and azimuth resolutions are 1.18 cm and 1.25 cm, respectively. The five types of civilian aircraft, as B747, B787, B777, DC10, and A320, are assumed for the target classification issue. Figure 4 shows the optical images of the five types of civilian aircraft.

5.1 Evaluation of Target Area Extraction

This subsection investigates the accuracy of target area extraction by the proposed method. Here, area in which the target exists is extracted by binarizing the SAR image, where the binalization threshold is determined by Otsu's discriminant analysis method [9]. For simulating the receiver

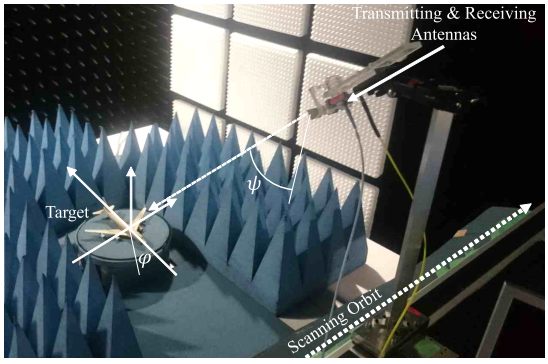

Fig. 3 Experimental setup.

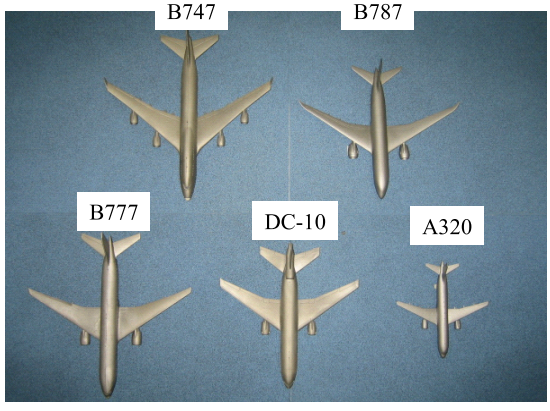

Fig. 4 Optical images of five civil aircraft models.

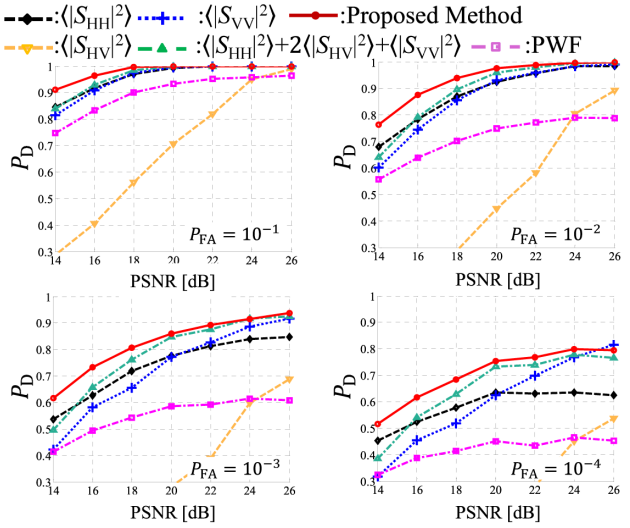

Fig. 5 Relationship between PSNR and detection probability P_{D} at $\phi = 0^\circ$ for each false alarm rate P_{FA}.

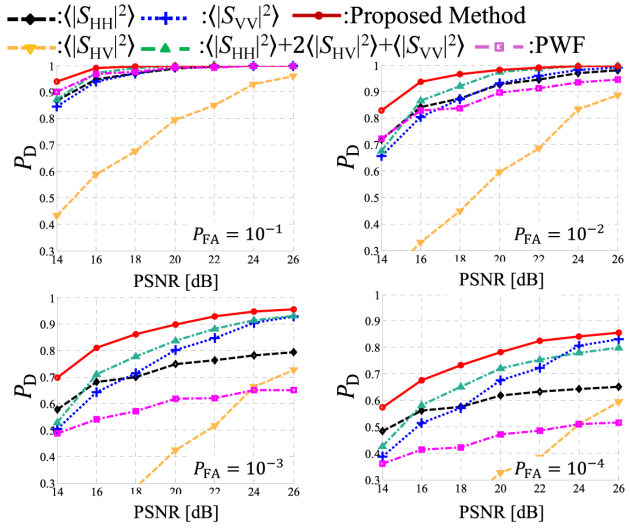

Fig. 6 Relationship between PSNR and detection probability P_{D} at $\phi = 15^\circ$ for each false alarm rate P_{FA}.

noise, white Gaussian noise is added numerically to the received signal. Figures 5 and 6 show PSNR versus the detection probability P_{D} for each the false-alarm rate P_{FA}, where the azimuth angle of the target ϕ is 0° and 15°, respectively. P_{D} is averaged with five aircraft cases for each P_{FA}. Figure 5 indicates that the detection probability P_{D} of the HV polarization image decreases significantly at low PSNR because the PSNR of HV polarization becomes the lowest in all polarization images in all P_{FA} cases. For reference, Table 1 shows the PSNR (defined in Eq. (9)) comparison for each polarization, where the average PSNR is around 18 dB. This table shows that the SNR of HV component is lowest in all types of aircraft, which degrades the accuracy for target area extraction. Furthermore, the detection accuracy with PWF also significantly degrades, compared with that obtained by the proposed method. This degradation is ascribed to the fact that the power of the target area is also suppressed through the decorrelating process in PWF method, and also this method does not consider the SNR imbalance in synthesizing the feature values. On the contrary, the proposed method provides most accurate target area extraction performance, compared with other all synthesizing methods. Figure 6 denotes the same evaluation in the case of the target rotating in azimuth direction as $\phi = 15^\circ$. In this case, the proposed method also outperforms for all combination methods, and indicates a well-robustness for the target rotating situations.

Table 1 PSNRs [dB] for each airplane in the experiment after an white Gaussian noise is added to data numerically.

	B747	B787	B777	DC10	A320	AVE
HH	25.5	17.9	21.5	24.5	19.7	21.8
VV	26.1	19.6	20.4	21.8	17.5	21.1
HV	13.1	13.6	13.4	17.5	14.6	14.4

5.2 Performance Evaluation for Classification

This subsection investigates the classification performance of the proposed method. At first, the power ratio variation of each polarization basis is investigated as follows. Figures 7 and 8 show the RGB synthesized SAR images (as $|S_{\mathrm{HH}}|+2|S_{\mathrm{HV}}|+|S_{\mathrm{VV}}|$) on LP basis at $\phi = 0^\circ$ and 30°, respectively. As shown these figures, the RBG color balance for the same target area is considerably changed due to azimuth rotation angle difference, which possibly degrades the classification performance in the method [3]. On the contrary, Figs. 9 and 10 show the RGB synthesized SAR images (as $|S_{\mathrm{LL}}|+2|S_{\mathrm{LR}}|+|S_{\mathrm{RR}}|$) on CP basis at $\phi = 0^\circ$ and 30°, respectively. These figures show that the RBG color balance in CP is apparently similar in terms of the target rotation. For more specific comparison, Figs. 11 and 12 illustrate the power ratio comparison of different azimuth angles, Here, the power ratio is investigated and averaged in the red marked region in Fig. 5, at $\phi = 0^\circ$ and 30°, respectively. This comparison shows that, while the power ratio of each LP basis components considerably changes according to target rotation, that of CP basis components is almost invariant in this situation regardless of target types. It will contribute a beneficial effect on the classification performance, because our proposed method also evaluates the difference of the ratio of each component in the classification process.

Next, the target classification accuracies of the proposed method and other possible combinations are investigated as follows. The neuron size of the assumed SOM is set to 31×31 and the total number of training trials is set to $T_{\mathrm{som}} = 30$. The training data for each aircraft with $\phi = 0^\circ$ are used for generating the SOM, namely, the learning process. The unknown SAR images are investigated, where the rotating azimuth angle ϕ is varied for $-30^\circ \le \phi \le 30^\circ$ with the 2° interval. In the angle compensating process, the reference image $P^{\mathrm{bi}}_{\mathrm{ref}}(x, y, 0)$ is set to that obtained at B747 with $\phi = 0^\circ$. Table 2 shows the probabilities of correct clas-

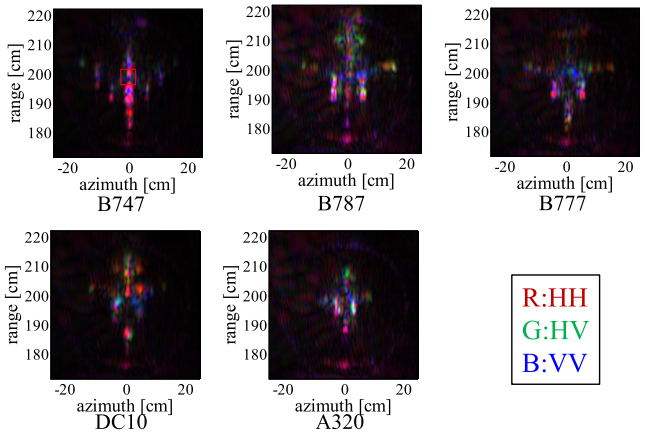

Fig. 7 RGB expression for SAR images on LP basis for each airplane at $\phi = 0°$.

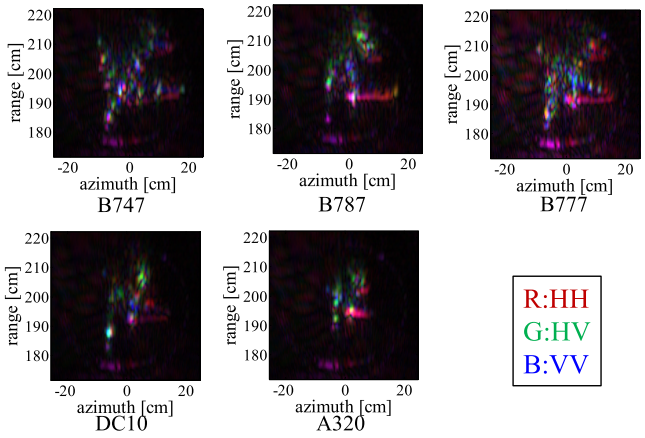

Fig. 8 RGB expression for SAR images on LP basis for each airplane at $\phi = 30°$.

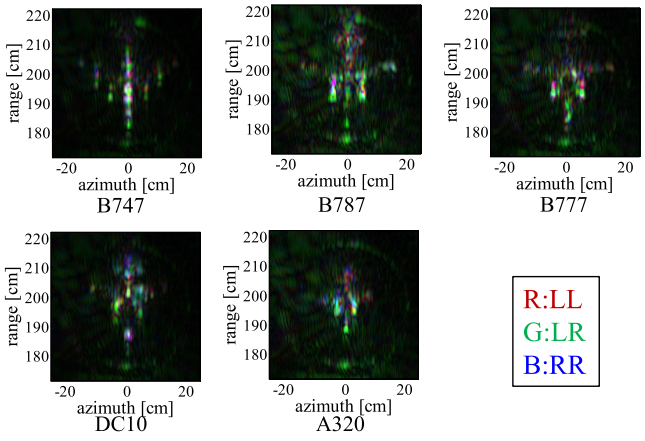

Fig. 9 RGB expression for SAR images on CP basis for each airplane at $\phi = 0°$.

sification for each method at the averaged PSNR = 32 dB, where no noise are added numerically to any SAR images. For each polarization basis, the feature value is employed as defined in Eq. (14). Here, the PSNR is averaged for all

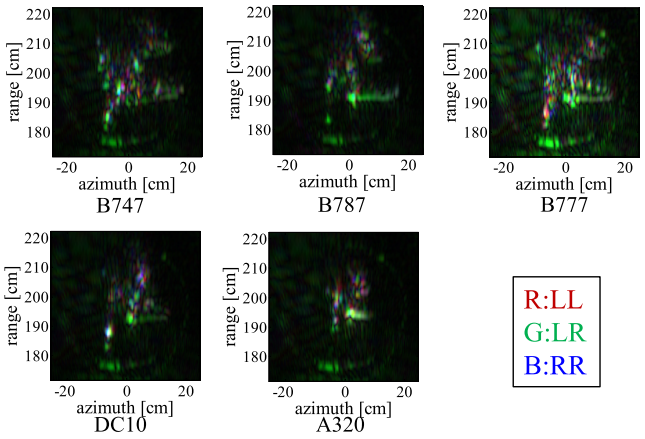

Fig. 10 RGB expression for SAR images on CP basis for each airplane at $\phi = 30°$.

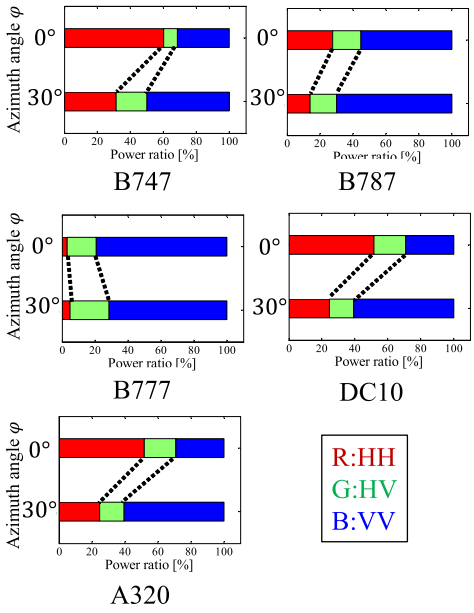

Fig. 11 Power ratio of LP basis in red marked area.

polarization and all targets. Table 3 summarizes the results in the case that the average PSNR is around 18 dB, where the white Gaussian noises are added numerically to the received signal for each polarization. For Table 3, these probabilities are averages for five different cases with different noise patterns. As shown in these tables, the full polarimetric exploitation denoted as LP or CP basis is effective for improving the ATR performance in terms of correct classification probability. Especially, the average probabilities of correct classification by the proposed method achieves the highest one in those of all single polarization data or the LP based full polaritric exploitation. This is because the feature value consisting of CP basis component is basically invariant for target rotation, and contributes the correct target classification by suppressing the undesirable changes of the feature values due to the target rotation. It should be

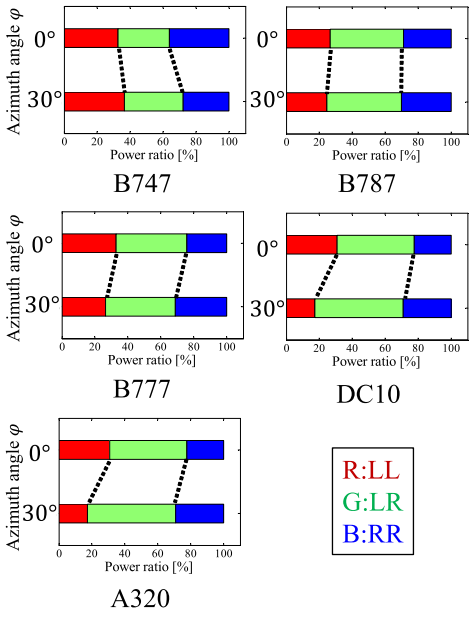

Fig. 12 Power ratio of CP basis in red marked area.

Table 2 Comparison of probability for correct classification at average PSNR = 32 dB.

		B747	B787	B777	DC10	A320	AVE
Single Pol.	HH	90 %	52%	97%	81%	42%	72%
	VV	90 %	65%	58%	97%	32%	68%
	HV	87%	39%	94%	55%	68%	68%
Full Pol.	LP	77%	42%	100%	68%	100%	77%
	CP	100%	42%	100%	97%	94%	87%

noted that the accuracy for classifying the B787 and A320 are not improved by using the proposed method, and is considerably lower compared with other target types in any data utilization. This is because there is a significant difference in SAR images between not rotating and rotating target case, which cannot be compensated by using only the image rotation of the training SAR image. It is considered that this difference depends on the target shape, where the multiple scattering effect may affect such image distortion. In addition, since the PSNRs of B787 and A320 are relatively lower than those of other targets as shown in Table 1, it is considered that, in such case, the randomness of additive noise affects the recognition accuracy more significantly. Also, the recognition process in any approaches, the unknown image is forcibly classified into some one among 5 target types. These facts also might cause a slight accuracy degradation of the proposed method, compared with the accuracy obtained by LP based approach, and should be addressed in the future work. Furthermore, since it was confirmed that the SAR image with rotation angle $\phi > 30°$ becomes considerably distorted and different from that with $\phi = 0°$, any feature vectors or recognition methods introduced in this paper could not achieve a correct recognition in such case. Consequently, we need more training data with different angle in order to expand the applicable range of rotation angles.

Table 3 Comparison of probability for correct classification at average PSNR = 18 dB.

		B747	B787	B777	DC10	A320	AVE
Single Pol.	HH	91%	42%	80%	80%	47%	68%
	VV	95%	54%	40%	41%	14%	49%
	HV	43%	24%	1%	47%	31%	29%
Full Pol.	LP	77%	40%	75%	75%	86%	70%
	CP	93%	36%	80%	80%	80%	74%

6. Conclusion

This paper extended the SOM based former method [7] so as to exploit full polarimetric SAR images. As pre-processing for classification issue, this paper proposes the target area extraction method based on the PSNR weighted synthesis of full polarimetric SAR images to improve the robustness to additive random noise by considering the SNR imbalance among data. In addition, the former SOM based ATR method is appropriately extended to full polarimetric data to be suitable for target rotating situation, where the target rotating angle estimation and CP basis conversion are newly introduced. The experimental validations, assuming the 1/100-scale X-band SAR model, demonstrated that our proposed method achieved the highest accuracy in terms of target area extraction and correct target classification, even under conditions of lower PSNR and angular varying situations. It is considered that this method maintains its effectiveness in other target shapes, which have horizontally expanded structures, such as ships or vehicles. However, in the case of target with vertically expanded structure, such as building, the image variance due to layover effect becomes more severe in target rotating, which could not be accurately compensated even by using the proposed method. This difficulty should be addressed in our future work by incorporating the layover effect compensation.

References

[1] B. Widrow, R.G. Winter, and R.A. Baxter, "Layered neural nets for pattern recognition," IEEE Trans. Acoust., Speech, Signal Processing, vol.36, no.7, pp.1109–1118, July 1988.
[2] X. Yu, Y. Li, and L.C. Jiao, "SAR automatic target recognition based on classifiers fusion," Proc. 2011 International Workshop on Multi-Platform/Multi-Sensor Remote Sensing and Mapping, pp.1–5, 2011.
[3] S. Kidera and T. Kirimoto, "Accurate and robust automatic target recognition method for SAR imagery with SOM-based classification," IEICE Trans. Commun., vol.E95-B, no.11, pp.3563–3571, Nov. 2012.
[4] F. Sadjadi, "Improved target classification using optimum polarimetric SAR signatures," IEEE Trans. Aerosp. Electron. Syst., vol.38, no.1, pp.38–49, Jan. 2002.
[5] G. Margarit, J.J. Mallorqui, J. Fortuny-Guasch, and C. Lopez-Martinez, "Exploitation of ship scattering in polarimetric SAR for an improved classification under high clutter conditions," IEEE Trans. Geosci. Remote Sens., vol.47, no.4, pp.1224–1235, April 2009.
[6] L.M. Novak, M.C. Burl, W. W. Irving, and G.J. Owirka, "Optimal polarimetric processing for enhanced target detection," NTC'91 — National Telesystems Conference Proceedings, pp.69–75, 1991.
[7] S. Ohno, S. Kidera, and T. Kirimoto, "Efficient SOM-based ATR

method for SAR imagery with azimuth angular variations," IEEE Geosci. Remote Sensing Lett., vol.11, no.11, pp.1901–1905, April 2014.
[8] H. Kimura, K.P. Papathanassiou, and I. Hajnsek, "Polarization orientation effects in urban areas on SAR data," Proc. 2005 IEEE International Geoscience and Remote Sensing Symposium, 2005. IGARSS'05., pp.4863–4867, 2005.
[9] N. Otsu, "A threshold selection method from gray-level histograms," IEEE Trans. Syst., Man, Cybern., vol.9, no.1, pp.62–66, Jan. 1979.
[10] H. Matsushita and Y. Nishio, "Batch-learning self-organizing map with false-neighbor degree between neurons," Proc. 2008 IEEE International Joint Conference on Neural Networks (IEEE World Congress on Computational Intelligence), pp.2259–2266, 2008.
[11] M. Ito, T. Miyoshi, and H. Masuyama, "The characteristics of the torus self organizing map," Proc. 6th International Conference on Soft Computing, pp.239–244, Fukuoka, Japan, 2000.
[12] A. Ultsch and H.P. Siemon, "Kohonen's self organizing feature maps for exploratory data analysis," Proc. International Neural Network Conference, pp.305–308, 1990.
[13] J.-S. Lee, D.L. Schuler, T.L. Ainsworth, E. Krogager, D. Kasilingam, and W.-M. Boerner, "On the estimation of radar polarization orientation shifts induced by terrain slopes," IEEE Trans. Geosci. Remote Sens., vol.40, no.1, pp.30–41, 2002.

Shouhei Ohno received his B.E. degree in Electronic Engineering from University of Electro-Communications in 2013 and M.E. degree at the Graduate School of Informatics and Engineering, University of Electro-Communications in 2015. He joined NEC Corporation in 2015.

Shouhei Kidera received his B.E. degree in Electrical and Electronic Engineering from Kyoto University in 2003 and M.I. and Ph.D. degrees in Informatics from Kyoto University in 2005 and 2007, respectively. He is currently an Associate Professor in Graduate School of Informatics and Engineering, the University of Electro-Communications, Japan. His current research interest is in advanced radar signal processing or electromagnetic inverse scattering issue for ultra wideband (UWB) sensor. He was awarded Ando Incentive Prize fo the Study of Electronics in 2012, Y oung Scientist's Prize in 2013 by the Japanese Minister of Education, Culture, Sports, Science and Technology (MEXT), and Funai Achievement Award in 2014. He is a member of the Institute of Electrical and Electronics Engineering (IEEE) and the Institute of Electrical Engineering of Japan (IEEJ).

Tetsuo Kirimoto received the B.S. and M.S. and Ph.D. degrees in Communication Engineering from Osaka University in 1976, 1978 and 1995, respectively. During 1978–2003 he stayed in Mitsubishi Electric Corp. to study radar signal processing. From 1982 to 1983, he stayed as a visiting scientist at the Remote Sensing Laboratory of the University of Kansas. From 2003 to 2007, he joined the University of Kitakyushu as a Professor. Since 2007, he has been with the University of Electro-Communications, where he is a Professor at the Graduate School of Informatics and Engineering. His current study interests include digital signal processing and its application to various sensor systems. Prof. Kirimoto is a senior member of IEEE and a member of SICE (The Society of Instrument and Control Engineers) of Japan.